

for each run of the spectrum by finding the intensity ratio of 14.4-keV  $\gamma$  rays and the other x rays and  $\gamma$  rays using the method suggested by Housley, Erickson, and Dash.<sup>10</sup> It should be noted that

Eq. (A1) strictly holds only if one charge state is present. However, since the intensity of  $\text{Fe}^{1+}$  resonance lines is much smaller than the  $\text{Fe}^{3+}$  lines, Eq. (A1) holds to a good approximation.

<sup>1</sup>J. H. Schulman and W. D. Compton, *Color Centers in Solids* (Pergamon, Oxford, 1963).

<sup>2</sup>G. D. Watkins, *Phys. Rev.* **113**, 79 (1959).

<sup>3</sup>W. Hayes, *Discussions Faraday Soc.* **26**, 58 (1958); S. C. Jain and K. Lal, in *International Conference on Science and Technology of Nonmetallic Crystals*, I. I. T. New Delhi, 1971 (unpublished); *Cryst. Lattice Defects* **1**, 165 (1970).

<sup>4</sup>S. Washimiya, *J. Phys. Soc. Japan* **18**, 1719 (1963); M. E. Hills, *ibid.* **19**, 760 (1964); M. Musa, *Phys. Status Solidi* **16**, 771 (1966); M. L. Reynolds, W. E. Hagston, and G. F. J. Garlik, *ibid.* **30**, 97 (1968).

<sup>5</sup>E. V. R. Sastry and T. M. Srinivasan, *Phys. Rev. B* **2**, 3415 (1970); *Phys. Status Solidi* **29**, K107 (1968).

<sup>6</sup>R. A. Andrews and Y. M. Kim, *Phys. Rev.* **154**, 220 (1967); **155**, 1029 (1967).

<sup>7</sup>S. V. Nistor and A. Darabont, *Solid State Commun.* **7**, 363 (1969); **8**, 451 (1970).

<sup>8</sup>M. De Coster and S. Amelinckx, *Phys. Letters* **1**, 245 (1962).

<sup>9</sup>J. G. Mullen, *Phys. Rev.* **131**, 1410 (1963).

<sup>10</sup>R. M. Housley, *Nucl. Instr. Methods* **35**, 77 (1965); R. M. Housley, N. E. Erickson, and J. G. Dash, *ibid.* **27**, 29 (1964).

<sup>11</sup>L. R. Walker, G. K. Wertheim, and V. Jaccarino,

*Phys. Rev. Letters* **4**, 412 (1960).

<sup>12</sup>F. Markham, in *F-Centers in Solids*, Suppl. 8 of *Solid State Physics*, edited by F. Seitz and D. Turnbull (Academic, New York, 1966).

<sup>13</sup>S. C. Jain, G. D. Sootha, and R. K. Jain, *J. Phys. C* **1**, 1220 (1968); R. K. Jain, Ph. D. thesis (Indian Institute of Technology, 1969) (unpublished).

<sup>14</sup>A. A. Maradudin, in *Solid State Physics*, edited by F. Seitz and D. Turnbull (Academic, New York, 1966), Vol. 18, p. 274.

<sup>15</sup>A. A. Maradudin, in *Proceedings of the First International Conference on Localized Excitation in Solids* (Plenum, New York, 1968).

<sup>16</sup>G. K. Wertheim and H. J. Guggenheim, *J. Chem. Phys.* **42**, 3873 (1965).

<sup>17</sup>V. I. Nikolaev and S. S. Yakirnov, *Zh. Eksperim. i Teor. Fiz.* **46**, 389 (1964) [*Sov. Phys. JETP* **19**, 264 (1964)].

<sup>18</sup>W. T. Berg and J. A. Morrison, *Proc. Roy. Soc. (London)* **A250**, 70 (1959).

<sup>19</sup>W. Triftshäuser and D. Schroerer, *Phys. Rev.* **187**, 491 (1969).

<sup>20</sup>R. H. Nussbaum, D. G. Howard, W. L. Nees, and C. F. Steen, *Phys. Rev.* **173**, 653 (1968).

## Symmetrized Multipulse Nuclear-Magnetic-Resonance Experiments in Solids: Measurement of the Chemical-Shift Shielding Tensor in Some Compounds\*

P. Mansfield, M. J. Orchard, D. C. Stalker, and K. H. B. Richards<sup>†</sup>

*Department of Physics, University of Nottingham, Nottingham, England*

(Received 17 April 1972)

An experimental study of the properties of one form of the three-state reflection-symmetry cycle is presented. The cycle and its compensated form are used to measure the chemical shielding tensor of  $^{19}\text{F}$  in polytetrafluoroethylene  $[(\text{C}_2\text{F}_4)_n]$ , and  $^{31}\text{P}$  in powdered zinc phosphide ( $\text{Zn}_3\text{P}_2$ ). The effect of phase errors is discussed and the principle of phase compensation is demonstrated in a phase-alternated sequence. Amplitude-modulation effects of phase errors are also discussed.

### I. INTRODUCTION

In most solids which have a nuclear-spin species the dominant spin-spin magnetic interaction is via the nuclear dipole-dipole coupling. It was recognized a long time ago<sup>1,2</sup> that high-speed rotation of the specimen about the so-called "magic axis" could substantially reduce the magnetic dipolar interaction tensor but not the isotropic parts of the chemical shift or shielding tensor or the isotropic part of the electron-coupled nuclear

pseudodipolar interaction or exchange interaction. Indeed, as with random motion in a mobile liquid, one obtains the familiar structured high-resolution spectra.

More recently,<sup>3-11</sup> it has been shown both theoretically and experimentally that irradiation of solids with certain multipulse sequences can also selectively remove or reduce the dipolar interaction thus revealing previously hidden and usually more interesting interactions in solids. This is because these smaller interactions reflect the

solid-state electronic structure around resonant nuclei whereas the pure static dipolar interaction carries information on the lattice structure. One important difference between multipulse and specimen rotation experiments is that in the former, since the specimen is at rest, all components of the chemical shielding tensor are present in the spectrum, whereas in the latter case only the isotropic value of the chemical shielding tensor is measured.

In almost all the multipulse work reported so far, the four-pulse cycle of Waugh, Huber, and Haeberlen<sup>4</sup> has been employed. Recently, however, some new cycles have been proposed by Mansfield<sup>12-14</sup> which are theoretically capable of greater line-narrowing efficiency in a dipolar-broadened solid with a chemical-shift distribution on "resonance." In these cycles, the dipolar interaction Hamiltonian is switched successively through three states and then by reflection symmetry back to the initial state.

In this paper we wish to report several experiments carried out with some of these new cycles using a computer-controlled pulse spectrometer. By way of example we have used these cycles to study the chemical-shift tensor of <sup>31</sup>P in powdered zinc phosphide (Zn<sub>3</sub>P<sub>2</sub>) and of <sup>19</sup>F in polytetrafluoroethylene [(C<sub>2</sub>F<sub>4</sub>)<sub>n</sub>], both at 77°K. The results are discussed in terms of the current theories of chemical shift. We also report experiments with variations on some older cycles which for convenience are illustrated on a liquid sample.

## II. REFLECTION-SYMMETRY CYCLES

In three-state reflection-symmetry cycles,<sup>12-14</sup> the interaction Hamiltonian is switched for equal times  $\tau$  through the three Hamiltonian states, 1, 2, 3, in the sequence 1, 2, 3, 3, 2, 1, where the numbers refer to the following Hamiltonian states:

$$\begin{aligned} \hbar H_1^1 = & \sum_{i < j} \hbar A_{ij} (\vec{I}_i \cdot \vec{I}_j - 3 I_{zi} I_{zj}) \\ & + \sum_i \hbar \delta_i I_{zi} + \sum_{i < j} \hbar \tilde{A}_{ij} \vec{I}_i \cdot \vec{I}_j, \quad (1a) \end{aligned}$$

$$\begin{aligned} \hbar H_1^2 = & \sum_{i < j} \hbar A_{ij} (\vec{I}_i \cdot \vec{I}_j - 3 I_{xi} I_{xj}) \\ & + \sum_i \hbar \delta_i I_{xi} + \sum_{i < j} \hbar \tilde{A}_{ij} \vec{I}_i \cdot \vec{I}_j, \quad (1b) \end{aligned}$$

$$\begin{aligned} \hbar H_1^3 = & \sum_{i < j} \hbar A_{ij} (\vec{I}_i \cdot \vec{I}_j - 3 I_{yi} I_{yj}) \\ & + \sum_i \hbar \delta_i I_{yi} + \sum_{i < j} \hbar \tilde{A}_{ij} \vec{I}_i \cdot \vec{I}_j, \quad (1c) \end{aligned}$$

where the dipolar interaction coupling constant is given by

$$A_{ij} = -\frac{1}{2} \gamma^2 \hbar P_{ij} \quad (2)$$

and

$$P_{ij} = 2P_2(\cos\theta_{ij})/\gamma_{ij}^3,$$

the terms in this expression having their usual meaning,  $\delta_i$  is the resonance shift of the  $i$ th spin due to chemical shielding and  $\tilde{A}_{ij}$  is the exchange interaction coupling constant. The switching is achieved by appropriately chosen and spaced resonant rf pulses. Since the labeling of the interaction Hamiltonian states is arbitrary, it is clear that there are six forms of the reflection-symmetry cycle only three of which are required to cover all permutations of the three states. We denote these reflection cycles in shorthand notation  $\llbracket 1, 2, 3 \rrbracket$ ,  $\llbracket 1, 3, 2 \rrbracket$ , and  $\llbracket 2, 1, 3 \rrbracket$  or alternatively  $\llbracket 3, 2, 1 \rrbracket$ ,  $\llbracket 2, 3, 1 \rrbracket$ , and  $\llbracket 3, 1, 2 \rrbracket$ . The various interaction Hamiltonian states may be achieved by applying 90° rf pulses, 120° rf pulses and/or video pulses which modulate the static magnetic field. For resonant 90° rf pulses, the simplest pulse-timing representations of the first three forms of the reflection-symmetry cycle are

$$\llbracket 1, 2, 3 \rrbracket$$

$$\equiv (\tau - P_x P_y - \tau - P_y - 2\tau - P_{-y} - \tau - P_y P_x - \tau),$$

$$\llbracket 2, 1, 3 \rrbracket$$

$$\equiv (P_{-y} - \tau - P_y - \tau - P_x - 2\tau - P_{-x} - \tau - P_{-y} - \tau - P_y),$$

$$\llbracket 1, 3, 2 \rrbracket$$

$$\equiv (\tau - P_x - \tau - P_{-y} - 2\tau - P_y - \tau - P_{-x} - \tau),$$

where  $P_{\pm\alpha}$  represents a 90° rf pulse applied along the  $\pm\alpha$  axis in the rotating reference frame. All three forms of the reflection-symmetry cycle together with the expected nuclear signal under particular initial conditions are sketched in Fig. 1.

These particular conditions are rather important in that they exploit the refocusing properties of solid echoes.<sup>15,16</sup> Furthermore, the magnetization is placed along the  $x$  and  $z$  rotating frame axes only, making the analogy between these experiments and the line-narrowing experiments similar to those described by Lee and Goldburg<sup>17</sup> more tenuous. In the multipulse analog of one form of their experiments,<sup>5</sup> the magnetization is made to sample the  $x$ ,  $y$ , and  $z$  axes for equal times. Although it has been shown theoretically<sup>14</sup> that a fully symmetrized cycle containing all three forms above is required for the greater efficiency in line narrowing, the simplest to produce experimentally is  $\llbracket 1, 3, 2 \rrbracket$  which in itself is theoretically more efficient than previous cycles of equal or lower rank. For this reason we shall confine ourselves almost exclusively to discussion and application of the  $\llbracket 1, 3, 2 \rrbracket$  cycle.

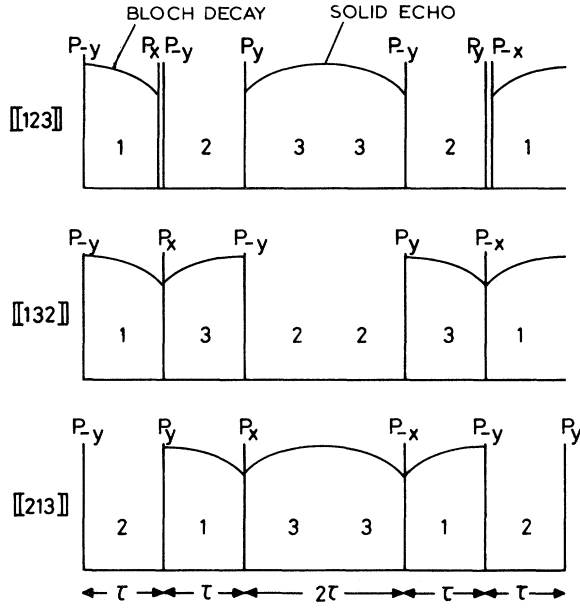


FIG. 1. Elementary forms of the three-state reflection-symmetry cycle. The expected signal response for particular initial conditions is also sketched in. As shown both  $\llbracket 1, 2, 3 \rrbracket$  and  $\llbracket 1, 3, 2 \rrbracket$  can be used in their own right, the spin system in each case being assumed in an initial equilibrium state. For  $\llbracket 2, 1, 3 \rrbracket$  as sketched, the spin system is assumed to be initially in a nonequilibrium state.

### A. Compensated Cycles

All three forms of the reflection-symmetry cycle can be compensated in first order for the impairing effects of finite rf pulse width  $t_w$ , rf inhomogeneity and deviation from the ideal  $180^\circ$  phase shift in a phase modulator common to both  $x$  and  $y$  pulses, as well as deviations from the ideal  $90^\circ$  phase shift implied in the  $x$  pulse. For compensation of the first two effects it has been shown<sup>14</sup> that one needs a cycle comprising two reflection-symmetry cycles, the second of which has the phases of the  $x$  pulses only shifted by  $180^\circ$ . Since this procedure has the effect of reversing the sign of the relevant linear term in the interaction Hamiltonian, we denote the compensated form of  $\llbracket 1, 3, 2 \rrbracket$  as  $\llbracket 1, 3, 2; 1, \bar{3}, 2 \rrbracket$ . Compensation of the  $\llbracket 2, 1, 3 \rrbracket$  cycle requires extra  $P_x$  pulses in the pulse-timing representation (see Ref. 14). We discuss the details of phase compensation later on.

### B. Effective-Chemical-Shift Hamiltonian

For the  $\llbracket 1, 3, 2 \rrbracket$  cycle, the average chemical-shift Hamiltonian over the  $6\tau$  period is

$$\bar{h}\bar{H}_c = \frac{1}{3} \sum_i \bar{h}\delta_i \left\{ (I_{xi} + I_{yi} + I_{zi}) \left[ 1 + \frac{t_w}{2\tau} \left( \frac{4}{\pi} - 1 \right) \right] \right.$$

$$\left. + \frac{t_w}{2\tau} \left( \frac{4}{\pi} - 1 \right) I_{yi} \right\}, \quad (3a)$$

which gives for the approximate effective chemical shift over the cycle

$$\delta_{i \text{ eff}} \approx (\delta_i / \sqrt{3}) [1 + (t_w/2\tau)(4/\pi - 1)]. \quad (3b)$$

For the compensated  $\llbracket 1, 3, 2; 1, \bar{3}, 2 \rrbracket$  cycle, the average chemical-shift Hamiltonian over the  $12\tau$  period is

$$\bar{h}\bar{H}_c = \frac{1}{3} \sum_i \bar{h}\delta_i [1 + (t_w/2\tau)(4/\pi - 1)] (I_{xi} + I_{zi}), \quad (4a)$$

which gives for the effective chemical shift over the compensated cycle

$$\delta_{i \text{ eff}} = \delta_i \frac{1}{3} \sqrt{2} [1 + (t_w/2\tau)(4/\pi - 1)]. \quad (4b)$$

### C. Signal and Baseline Response

In the interpretation of experimental multipulse response oscilloscope traces one is often presented with a complicated trace which includes "baseline" modulation. Previous analysis was concerned with signal response.<sup>14</sup> However, it is instructive and helpful in the interpretation of actual data to have some clear picture of the expected ideal full response. In this paper we restrict ourselves to a discussion of the two cycles  $\llbracket 1, 3, 2 \rrbracket$  and  $\llbracket 1, 3, 2; 1, \bar{3}, 2 \rrbracket$ . In each case we calculate the in-phase and quadrature components of magnetization  $\langle x(t) \rangle_s$  and  $\langle y(t) \rangle_s$  and the "baseline" response of each component  $\langle x(t) \rangle_0$  and  $\langle y(t) \rangle_0$  in the average Hamiltonian limit.<sup>3</sup> For the baseline response the averaging has to be performed over a differently defined cycle with consequently a different average Hamiltonian. Evolution over noncumulative periods which is ignored except for the effect of the rf pulses, introduces time-origin shifts  $\Delta t$  of  $3\tau$  and  $9\tau$  as indicated below. For  $\llbracket 1, 3, 2 \rrbracket$  we obtain

$$\langle x(t) \rangle_s = \frac{2}{3} \sum_i \cos(\delta_i t / \sqrt{3}) + \frac{1}{3}, \quad (5a)$$

$$\langle x(t) \rangle_0 = -\frac{2}{3} \sum_i \cos[(\delta_i / \sqrt{3})(t - 3\tau) - \frac{2}{3}\pi] - \frac{1}{3} \quad (5b)$$

and

$$\langle y(t) \rangle_s = \frac{2}{3} \sum_i \cos(\delta_i t / \sqrt{3} - \frac{2}{3}\pi) + \frac{1}{3}, \quad (5c)$$

$$\langle y(t) \rangle_0 = \frac{1}{3} \sum_i \cos[(\delta_i / \sqrt{3})(t - 3\tau) - \frac{4}{3}\pi] - \frac{1}{3}, \quad (5d)$$

where the time  $t = 6\tau n$ ,  $n$  integer.

For the compensated cycle  $\llbracket 1, 3, 2; 1, \bar{3}, 2 \rrbracket$  we obtain

$$\langle x(t) \rangle_s = \frac{1}{2} [1 + \sum_i \cos(\frac{1}{3}\sqrt{2} \delta_i t)], \quad (6a)$$

$$\langle x(t) \rangle_0 = - (1/\sqrt{2}) \sum_i \sin[\frac{1}{3}\sqrt{2} \delta_i (t - 3\tau)] + (1/\sqrt{2}) \sum_i \sin[\frac{1}{3}\sqrt{2} \delta_i (t - 9\tau)] \quad (6b)$$

and

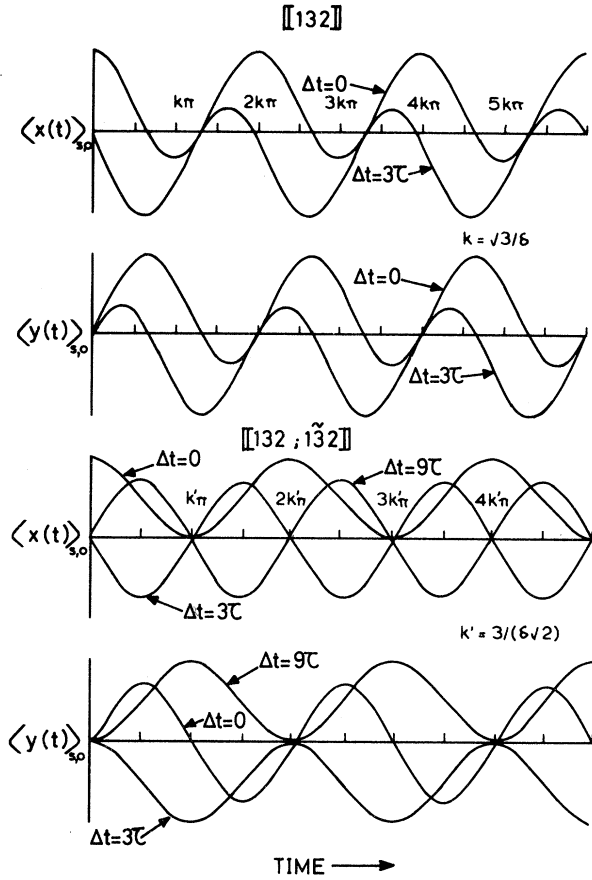


FIG. 2. Sketch of transverse response  $\langle x(t) \rangle_{s,0}$  and  $\langle y(t) \rangle_{s,0}$  in a noninteracting spin system for the ideal  $[[1, 3, 2]]$  and  $[[1, 3, 2; \bar{1}, \bar{3}, 2]]$  cycles considered in the limit  $\tau \rightarrow 0$  and shifted slightly above resonance. Note the "baseline" modulations  $\langle x(t) \rangle_0$  and  $\langle y(t) \rangle_0$ .

$$\langle y(t) \rangle_s = (1/\sqrt{2}) \sum_i \sin(\frac{1}{3}\sqrt{2} \delta_i t), \quad (6c)$$

$$\langle y(t) \rangle_0 = -\frac{1}{2} \{1 - \sum_i \cos[\frac{1}{3}\sqrt{2} \delta_i (t - 3\tau)]\} + \frac{1}{2} \{1 - \sum_i \cos[\frac{1}{3}\sqrt{2} \delta_i (t - 9\tau)]\}, \quad (6d)$$

where the time  $t = 12\tau n$ ,  $n$  integer.

These results are summarized schematically in Fig. 2 and illustrate the general complexity of the response if studied visually on an oscilloscope.

Since the anisotropic part of the chemical-shift tensor remains in these experiments the effective line shape that we expect would in general be asymmetric. This means that in taking Fourier transforms of the transverse response one should perform the full cosine and sine transform on the in-phase and quadrature components of signal, respectively. We discuss this in more detail later on in Sec. IID. From Eqs. (5a) and (5c) we note that full Fourier transforms can only be performed if the constants are subtracted and the data have a common normalization. An interesting result from

Eq. (5b) is that in the limit  $\tau \rightarrow 0$  the  $\langle x(t) \rangle_0$  baseline signal component actually contains all the information necessary for a sine transform. To extract the useful information from  $\langle x(t) \rangle_0$  one requires very accurate data, since the quantity  $\langle x(t) \rangle_s + \langle x(t) \rangle_0$  is required in the computation which involves baseline differences. Our own preliminary efforts with single shot data have not been very successful. However, meaningful results could be obtained with signal averaged data. Simultaneous observation of both  $\langle x(t) \rangle_s$  and  $\langle y(t) \rangle_s$  would, of course, allow a direct procedure for full Fourier transforms. However, as we discuss later on, this is actually unnecessary if the transverse response is observed off-resonance.

#### D. Fourier Transformation

The transverse response function  $f(t)$  is related to the complex susceptibility of the  $i$ th component of an inhomogeneously broadened line by the Fourier integral expression<sup>18,19</sup>

$$f(t) = -\frac{1}{2} \gamma K \sum_i \int_{-\infty}^{\infty} \left[ -i\pi \delta(\Delta\omega_{0i} + \Delta\omega) + \mathcal{P} \left( \frac{1}{\Delta\omega_{0i} + \Delta\omega} \right) \right] \times e^{-i\Delta\omega t} d(\Delta\omega), \quad (7a)$$

where  $\mathcal{P}$  denotes the Cauchy principal part of the integral and  $\Delta\omega_{0i}$  is the resonance shift of the  $i$ th spin from its unshielded value. The constant  $K$  is given by

$$K = 2\omega_0 N I(I+1)/3kT, \quad (7b)$$

where  $N$  is the total number of spins,  $\omega_0$  is the unshielded Larmor angular frequency,  $I$  is the spin number,  $k$  is Boltzmann's constant, and  $T$  the absolute temperature. Integration of Eq. (7a) gives for the transverse response in the absence of dipolar line broadening

$$f(t) = -\frac{1}{2} \gamma K \Theta(t) \{ \sum_i \cos(\Delta\omega_{0i} t) + i \sin(\Delta\omega_{0i} t) \} = x(t) + iy(t), \quad (8a)$$

where the step function  $\Theta(t)$  is defined as

$$\Theta(t) = 1, \quad t > 0 \\ = 0, \quad t < 0. \quad (8b)$$

Now for a symmetric distribution of chemically shifted spins the summation over the  $\sin(\Delta\omega_{0i} t)$  term vanishes for  $t > 0$  but does not vanish for an asymmetric distribution. Clearly, therefore, in regenerating the absorption line shape from the transverse response function one should include both the  $x(t)$  and  $y(t)$  components of the transverse response and perform the full cosine and sine transform:

$$\chi''(\Delta\omega) = \int_{-\infty}^{\infty} [x \cos(\Delta\omega t) + y \sin(\Delta\omega t)] dt. \quad (9)$$

Neglect of the  $y(t)$  component clearly always will give a symmetric line on or off the "resonance" condition. For example, if we move off-resonance by imposing a bias of angular frequency  $\Omega$ , the absorption line, neglecting the sine transform, is from the above discussion

$$\chi''(\Delta\omega) = -\frac{1}{2}\gamma K \sum_i \delta(\Delta\omega + \Delta\omega_{0i} + \Omega) + \delta(\Delta\omega - \Delta\omega_{0i} - \Omega). \quad (10)$$

We see therefore that although the summation over the inhomogeneous distribution may be asymmetric about  $\pm\Omega$ , the over-all line transform is still symmetric about  $\omega_0$ . The neglected  $y(t)$  component holds information on the *phase* so that the full transform would automatically select the correct side of the above line-shape equation (10) corresponding to an arbitrary shift  $\pm\Omega$ . If the  $x(t)$  component alone is to be used for asymmetric lines the correct sign of  $\Omega$  must be determined experimentally, that is, by purposely shifting off-resonance above or below by some angular frequency  $\Omega$  large enough to give resolution of the doublet about  $\omega_0$ . This condition is satisfied if  $\Omega > \Delta\omega_{0i(\max)}$ . As a cautionary remark we note that in seeking to satisfy this last inequality one must be sure that another is not violated, namely, the condition on the cycle itself that it will register rapid oscillations. To ensure this, one must simultaneously satisfy the condition

$$\pi/(\Omega + \Delta\omega_{0i(\max)}) > n\tau,$$

where  $n\tau$  is the relevant cycle time. Because of this constraint, in some cases, it may be better experimentally to work on "resonance," i. e., at a field close to the isotropic value of the chemical shift.

### III. EXPERIMENTAL DETAILS

#### A. Alignment Procedure

All initial pulse length and phase alignment is performed on  $^1\text{H}$  in  $\text{H}_2\text{O}$ ,  $^{19}\text{F}$  in  $\text{C}_6\text{F}_6$ , or  $^{31}\text{P}$  in  $\text{H}_3\text{PO}_4$  liquid samples. The  $90^\circ$  pulses for the  $x$  and  $y$  channel are adjusted separately. This is done by adjusting the response to trains of  $x$  and  $y$  pulses in turn to give what we call the "double-triangle" pattern on resonance using a phase-sensitive detector. The  $90^\circ$  phase shifts are set maximizing the transverse  $\langle x(t) \rangle$  component in a  $P_{-y} - (\tau - P_x - \tau)_n$  sequence. The  $180^\circ$  phase shift is adjusted for a monotonic decay in a  $P_{-y} - (\tau - P_x - 2\tau - P_x - \tau)_n$  sequence. For reflection-symmetry cycles final fine adjustments to pulse width and transmitter output stage tuning are made to give a monotonic liquid inhomogeneous decay on resonance. Correct alignment is determined by attainment of symmetric oscillatory behavior about

the resonance condition. This alignment is further checked and adjusted until the correct scaling factors are obtained as discussed below.

#### B. Scaling Factors

In our experiments on fluorine and hydrogen the  $90^\circ$  pulse length was  $1.1 \mu\text{sec}$ . For  $\tau = 8.0 \mu\text{sec}$ , the departure from the ideal scaling factor of  $1/\sqrt{3} = 1/1.73$  in  $\llbracket 1, 3, 2 \rrbracket$  is significant and gives  $1/1.705$ , Eq. (3b). In the case of  $\llbracket 1, 3, 2; 1, \bar{3}, 2 \rrbracket$  departure from the ideal value of  $\frac{1}{3}\sqrt{2} = 1/2.12$  gives  $1/2.08$ , Eq. (4b). The experimental scaling factors obtained for  $\llbracket 1, 3, 2$  and  $\llbracket 1, 3, 2; 1, \bar{3}, 2 \rrbracket$  were  $1/1.69$  and  $1/1.96$ , respectively. Figure 3 shows the response to a  $\llbracket 1, 3, 2; 1, \bar{3}, 2 \rrbracket$  cycle in  $\text{C}_6\text{F}_6$  off-resonance. The latter section of the trace includes the normal free-induction decay for comparison. In our experiments on phosphorus the  $90^\circ$  pulse length was  $2.2 \mu\text{sec}$ . For  $\tau = 9.6 \mu\text{sec}$  and in the  $\llbracket 1, 3, 2 \rrbracket$  cycle the theoretical scaling factor is  $1/1.69$ , while the experimental value recorded was  $1/1.70$ .

#### C. Resonance Shifts

The multipulse experiments in solids involve moving off-resonance by some predetermined

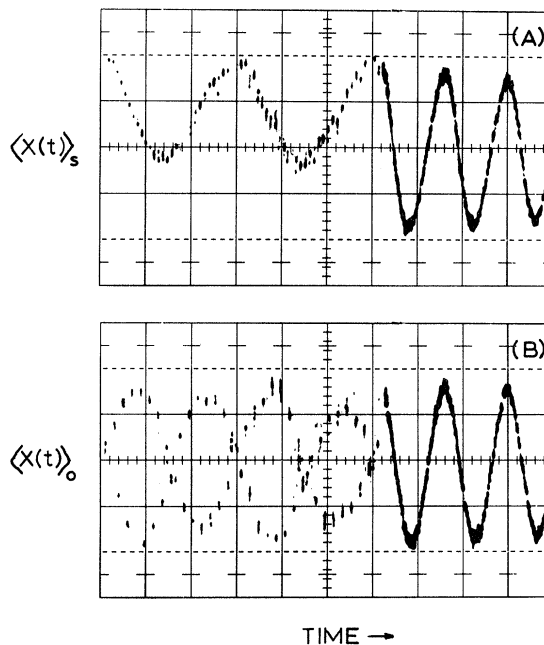


FIG. 3. Photographs of the response of  $^{19}\text{F}$  to the  $\llbracket 1, 3, 2; 1, \bar{3}, 2 \rrbracket$  cycle in liquid  $\text{C}_6\text{F}_6$  shifted  $0.37 \text{ G}$  from resonance. (a)  $\langle x(t) \rangle_s$  response only,  $\langle x(t) \rangle_0$  suppressed, (b)  $\langle x(t) \rangle_0$  response only,  $\langle x(t) \rangle_s$  suppressed. The horizontal sweep is  $0.5 \text{ msec}/\text{large division}$  and  $\tau = 8.0 \mu\text{sec}$  in both traces. Note that in both photographs the multipulse sequence is switched off at  $3.1 \text{ msec}$  and the subsequent signal is the ordinary free-induction decay.

amount. For both fluorine and phosphorus this was done by first obtaining the free-induction decay of the reference compound at the sample site. The Varian Fieldial was then calibrated above and below the resonance point by measuring the beat frequency on the free-induction decay of a liquid. We found that field calibrations made at room temperature were not reliable when extended to low temperatures, and it was necessary to calibrate at the actual working temperature.

A reliable way of achieving this was to quickly lower a small phial of the reference liquid into the liquid-nitrogen bath. Since it takes about 30 sec for the liquid sample to freeze solid, we found there was plenty of time when initially lowered to observe good liquid signal decays. Clamps on the sample rod and the reference liquid tube ensured reasonably accurate replacement of the samples to the same place in the magnet each time and thus guaranteed reproducible shifts to within about  $\pm 10\%$ .

#### D. Line-Narrowing Efficiency "On-Resonance"

A comparison of the line-narrowing efficiency between the  $\llbracket 1, 3, 2 \rrbracket$  cycle and its compensated form  $\llbracket 1, 3, 2; 1, \bar{3}, 2 \rrbracket$  was made "on-resonance" in  $(C_2F_4)_n$  at 298 and 77 °K. The alignment procedure was as follows: First the static magnetic field was adjusted to give the longest monotonic response for the  $\llbracket 1, 3, 2 \rrbracket$  cycle using a phase-sensitive detector. With no further adjustments both the  $\llbracket 1, 3, 2 \rrbracket$  and  $\llbracket 1, 3, 2; 1, \bar{3}, 2 \rrbracket$  cycle responses were recorded photographically. Of course the pulse widths and scaling factors, etc., were previously set up as described earlier using liquid perfluorobenzene. The results for 298 °K are shown in Fig. 4. Treating the decays as exponential we find the ratio of the time constants to be 2.7 at 298 °K, and at 77 °K the corresponding ratio is found to be 3.0. In each case the theoretical ratio based on just the scaling factors is 1.225 for  $\tau = 8.0 \mu\text{sec}$ . We conclude, therefore, that the first-order terms introduced into the average Hamiltonian by the finite  $90^\circ$  pulse length of  $1.1 \mu\text{sec}$  and the rf inhomogeneity are primarily responsible for the observed damping in the  $\llbracket 1, 3, 2 \rrbracket$  cycle on resonance. In both cycles off-resonance the experimental ratio is only slightly greater than the theoretical ratio mentioned above, suggesting an additional averaging mechanism no doubt similar to that discussed recently by Haeberlen, Ellett, and Waugh<sup>20</sup> for their nonsymmetrized four-pulse cycle. We hope to report elsewhere a more detailed comparative study of damping in various symmetrized cycles which is presently in progress on  $^{19}\text{F}$  in a single crystal of calcium fluoride. However, preliminary results for the  $\llbracket 1, 3, 2; 1, \bar{3}, 2 \rrbracket$  cycle with  $\tau = 8.0 \mu\text{sec}$  and the static magnetic field along the  $[111]$  crystal axis indicate a residual linewidth on resonance of about

230 Hz between the half-height points. Moving off-resonance gives a linewidth of about 190 Hz. Preliminary results on protons in the liquid crystal *p*-methoxy benzylidene-*p*-*n*-butyl aniline (MBBA) which, in the nematic phase, shows a featureless broad line of similar width to  $\text{CaF}_2$ , yields a residual linewidth of about 150 Hz for the  $\llbracket 1, 3, 2; 1, \bar{3}, 2 \rrbracket$  cycle with  $\tau = 8.0 \mu\text{sec}$ . The residual broadening functions used in the convolution integral to fit our spectra (Sec. IV) were substantially broader being 1.287 kHz for  $(C_2F_4)_n$ , corresponding approximately to Fig. 4(a), and a half of this value for zinc phosphide.

## IV. CHEMICAL-SHIFT STUDIES IN SOLIDS

### A. Shielding Tensor

The chemical-shift Hamiltonian in the laboratory reference frame in its most general form is given by<sup>21</sup>

$$\hbar H_c = \hbar \sum_i \gamma_i \bar{I}^i \cdot \bar{\sigma}^i \cdot \bar{H}, \quad (11)$$

where  $\bar{I}$  is the total spin vector,  $\bar{H}$  is the applied static magnetic field vector, the two being coupled by the chemical shielding tensor or dyadic for the  $i$ th spin  $\bar{\sigma}^i$ . This is formed from its second-rank tensor  $\sigma^i$  having, in general, nine components. If we take the applied field to be along the  $z$  axis, that

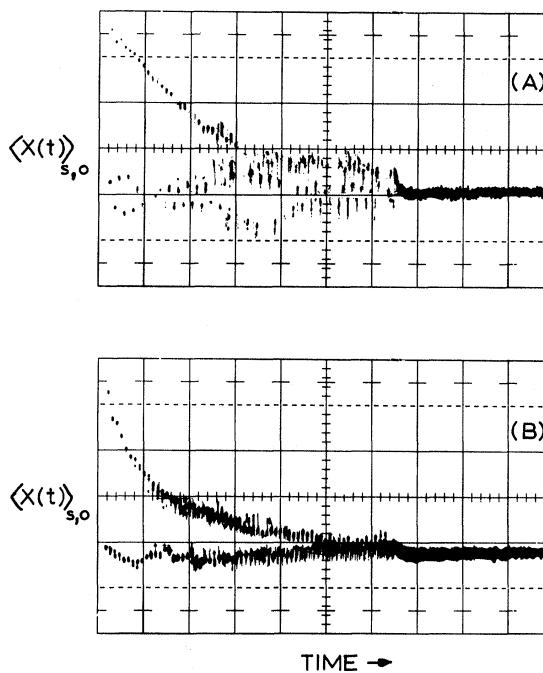


FIG. 4. Photographs of the  $^{19}\text{F}$  signals in  $(C_2F_4)_n$  at 293 °K in response to the following cycles applied at resonance: (a)  $\llbracket 1, 3, 2; 1, \bar{3}, 2 \rrbracket$ , (b)  $\llbracket 1, 3, 2 \rrbracket$ . In both cycles  $\tau = 8.0 \mu\text{sec}$  and for both traces the horizontal sweep is 0.5 msec/large division.

is  $\vec{H}(0, 0, H_0)$  then the shift Hamiltonian for similar spins becomes

$$\hbar H_c = \hbar \gamma \sum_i (I_{xi} \sigma_{xz}^i + I_{yi} \sigma_{yz}^i + I_{zi} \sigma_{zz}^i) H_0. \quad (12)$$

If we may further neglect the terms containing  $\sigma_{xz}^i$  and  $\sigma_{yz}^i$ , since the effect of these terms in the rotation frame is likely to be quite small, we have

$$H_c \approx \gamma \sum_i I_{zi} \sigma_{zz}^i H_0. \quad (13)$$

### 1. Principal-Axes System

The laboratory axes components of the shielding tensor may be expressed in terms of the diagonal

$$R(\alpha, \theta, \phi) = \begin{bmatrix} \cos \alpha \cos \phi - \cos \theta \sin \phi \sin \alpha & \cos \alpha \sin \theta + \cos \theta \cos \phi \sin \alpha & \sin \alpha \sin \theta \\ -\sin \alpha \cos \phi - \cos \theta \sin \phi \cos \alpha & -\sin \alpha \sin \theta + \cos \theta \cos \phi \cos \alpha & \cos \alpha \sin \theta \\ \sin \theta \sin \phi & -\sin \theta \cos \phi & \cos \theta \end{bmatrix}. \quad (14c)$$

Thus from Eqs. (13) and (14a)–(14c) we obtain for  $\sigma_{zz}^i$

$$\sigma_{zz}^i = \sin^2 \theta (\sin^2 \alpha) \sigma_{11}^i + \sin^2 \theta (\cos^2 \alpha) \sigma_{22}^i + (\cos^2 \theta) \sigma_{33}^i. \quad (15)$$

### 2. Isotropic Average

In the case of isotropic reorientation as in a liquid the average value of each of the angular coefficients in Eq. (15) is  $\frac{1}{3}$  so that the isotropic part of the chemical-shift tensor is

$$\bar{\sigma}_{zz}^i = \frac{1}{3} \text{Tr} \underline{\sigma}^i = \frac{1}{3} (\sigma_{11}^i + \sigma_{22}^i + \sigma_{33}^i). \quad (16)$$

### 3. Axial Symmetry

If the shielding tensor has axial symmetry then we may set  $\sigma_{11} = \sigma_{22} = \sigma_{\perp}$  and  $\sigma_{33} = \sigma_{\parallel}$ , for example, in which case

$$\sigma_{zz} = \sigma_{\perp} \sin^2 \theta + \sigma_{\parallel} \cos^2 \theta. \quad (17)$$

Clearly this may be expressed in terms of the isotropic chemical shift, Eq. (16), and a traceless part in which case for  $\sigma_{\parallel} = -2\sigma_{\perp}$  one obtains

$$\sigma_{zz} = \frac{1}{3} \text{Tr} \underline{\sigma} - \sigma_{\perp} (3 \cos^2 \theta - 1). \quad (18)$$

For a powder of isotropically oriented crystallites and in the absence of dipolar or other sources of line broadening, Bloembergen and Rowland<sup>23,24</sup> have shown that for small relative shifts, Eq. (18) leads to the line-shape expression

$$g(\omega) = \frac{1}{2} (\omega_{\parallel} - \omega_{\perp})^{-1/2} (\omega - \omega_{\perp})^{-1/2} \quad (19a)$$

for  $\omega_{\perp} < \omega < \omega_{\parallel}$ . They also give a general expression for the line shape when the shielding tensor does not have axial symmetry. In this case

$$g(\omega) = \pi^{-1} (\omega - \omega_{33})^{-1/2} (\omega_{11} - \omega_{22})^{-1/2} K(x), \quad (19b)$$

with

tensor representation or principal-axes system by the transformation

$$\underline{\sigma}^L = R^{\dagger} \underline{\sigma}^P R, \quad (14a)$$

where

$$\underline{\sigma}^P = \begin{bmatrix} \sigma_{11} & & \\ & \sigma_{22} & \\ & & \sigma_{33} \end{bmatrix}. \quad (14b)$$

The rotation or transformation matrix  $R(\alpha, \theta, \phi)$  corresponding to rotation through the Euler angles  $\alpha, \theta, \phi$  is given by<sup>22</sup>

$$x^2 = \frac{(\omega_{22} - \omega_{33})(\omega_{11} - \omega)}{(\omega_{11} - \omega_{22})(\omega - \omega_{33})} \quad \text{for } \omega_{11} > \omega > \omega_{22}$$

and

$$g(\omega) = \pi^{-1} (\omega_{11} - \omega)^{-1/2} (\omega_{22} - \omega_{33})^{-1/2} K(x), \quad (19c)$$

with

$$x^2 = \frac{(\omega - \omega_{33})(\omega_{11} - \omega_{22})}{(\omega_{11} - \omega)(\omega_{22} - \omega_{33})} \quad \text{for } \omega_{22} > \omega > \omega_{33}$$

and also

$$g(\omega) = 0 \quad \text{for } \omega > \omega_{11} \text{ or } \omega < \omega_{33}. \quad (19d)$$

Here  $K(x)$  is the tabulated complete elliptic integral.

In practice there is always some additional residual line broadening described by the function  $f(\omega)$ . This may be included in the over-all line shape  $G(\omega)$  by convoluting with the ideal powder pattern  $g(\omega)$ , thus

$$G(\omega) = \int_{-\infty}^{\infty} g(\omega') f(\omega - \omega') d\omega'. \quad (20)$$

## 4. Molecular Axes System

The principal components of the shielding tensor will not, in general, coincide with the molecular axes  $i, j, k$ . The tensor components in this frame will of course be related by a tensor transformation and can be deduced from single-crystal studies. Mehring *et al.*<sup>10</sup> have shown that in solids with certain types of anisotropic motion the orientation of the chemical-shift tensor with respect to the molecular frame can be assigned.

### B. Experimental Results

#### 1. Polytetrafluoroethylene

We have studied polytetrafluoroethylene ( $C_2F_4$ )<sub>n</sub> at 77 °K using the compensated [1, 3, 2; 1,  $\frac{2}{3}$ , 2]

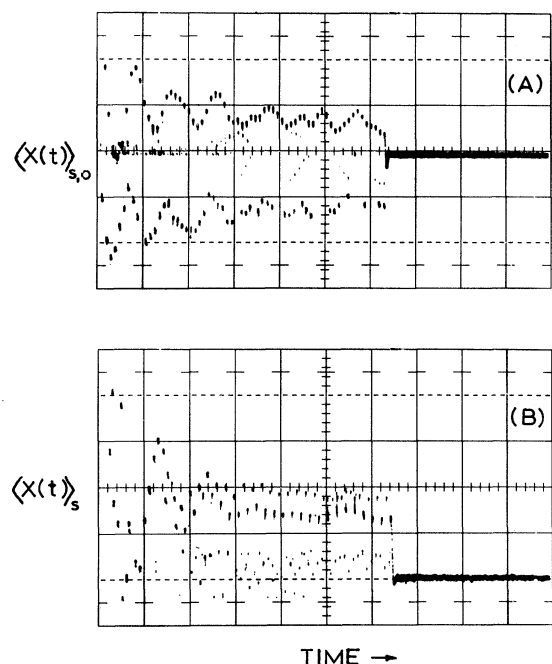


FIG. 5. Photographs of the  $^{19}\text{F}$  signals in  $(\text{C}_2\text{F}_4)_n$  at  $77^\circ\text{K}$  in response to the following cycles applied off-resonance by  $\Delta H = 1.2\text{ G}$ : (a)  $[[1, 3, 2]]$  showing  $\langle x(t) \rangle_s$  and  $\langle x(t) \rangle_0$  signals, (b)  $[[1, 3, 2; 1, 3, 2]]$  showing  $\langle x(t) \rangle_s$  only with  $\langle x(t) \rangle_0$  suppressed. In both cycles  $\tau = 8.0\ \mu\text{sec}$  and for both traces the horizontal sweep is  $0.5\ \text{msec}/\text{large division}$ .

cycle slightly shifted off-resonance and with  $\tau = 8.0\ \mu\text{sec}$ . The data taken at  $9.0\ \text{MHz}$  were recorded photographically. As a comparison, the photographic traces of both the uncompensated and compensated forms of the cycle are reproduced in Fig. 5.

Fourier transformation of the data points in Fig. 5(b) sampled once per cycle is presented in Fig. 6(a) with the frequency scaling factor removed. Our results confirm the previously reported chemical-shift anisotropy of Mehring *et al.*<sup>10</sup> measured on powdered  $(\text{C}_2\text{F}_4)_n$  at  $81^\circ\text{K}$  using the nonsymmetric uncompensated four-pulse cycle.<sup>4</sup> Our sample was

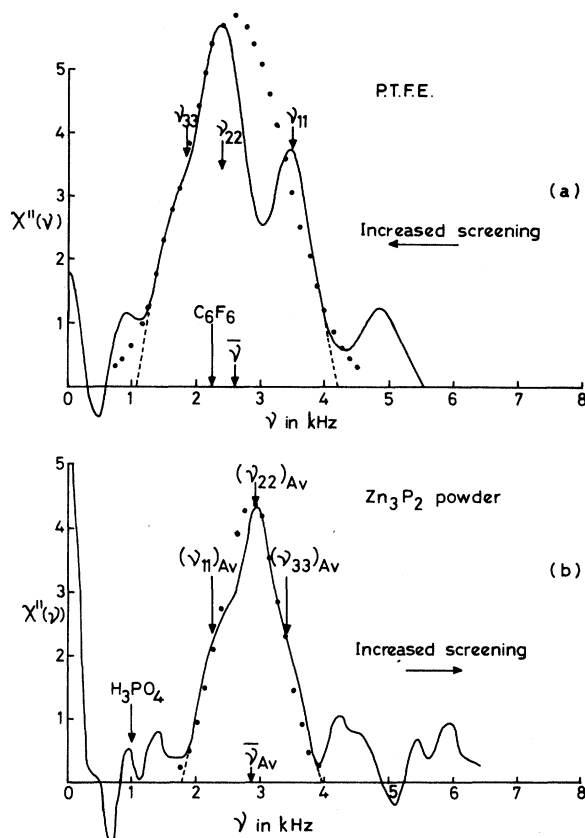


FIG. 6. Fourier-transformed line shapes of multipulse response signals sampled once per cycle from data similar to Fig. 5(b) for  $(\text{C}_2\text{F}_4)_n$  and Fig. 7 for  $\text{Zn}_3\text{P}_2$ . Frequency scaling factors have been removed. (a)  $(\text{C}_2\text{F}_4)_n$  extruded rod at  $77^\circ\text{K}$ , (b)  $\text{Zn}_3\text{P}_2$  powder at  $77^\circ\text{K}$ . The dotted line indicates truncation of the spectral width in both (a) and (b). The closed circles are the theoretical powder line shape, Eqs. (19b)–(19d) and (20).

commercial grade extruded rod. Partial alignment of the molecular chains along the extrusion axis would cause deviations from the isotropic powder pattern and may be responsible for the dip in our spectrum at  $3\ \text{kHz}$ . From our data, we are able to estimate the mean chemical shift with

TABLE I. Mean chemical shift with respect to the stated liquid reference compound and the traceless components of the anisotropic shielding tensor.

Substance	Traceless shift tensor components (ppm)			Isotropic shift (ppm)	Reference compound
	$\Delta\sigma_{11}$	$\Delta\sigma_{22}$	$\Delta\sigma_{33}$	$\bar{\sigma}$	
$(\text{C}_2\text{F}_4)_n$	-100	22	78	-39	$\text{C}_6^{19}\text{F}_6$
	$(\Delta\sigma_{11})_{av}$	$(\Delta\sigma_{22})_{av}$	$(\Delta\sigma_{33})_{av}$	$\bar{\sigma}_{av}$	
$\text{Zn}_3\text{P}_2$	-67	6	61	210	85% aqueous solution $\text{H}_3^{31}\text{PO}_4$

respect to liquid perfluorobenzene and the traceless components of the anisotropic shielding tensor. These values are given in Table I.

## 2. Zinc Phosphide

Phosphorus in powdered zinc phosphide ( $\text{Zn}_3\text{P}_2$ ) has been the subject of several previous NMR studies by the spinning solid method.<sup>25,26</sup> In these studies a pair of lines of equal intensity was observed with chemical shifts  $\bar{\sigma}_1$  and  $\bar{\sigma}_2$ . The average shift  $\bar{\sigma}_{\text{av}} = \frac{1}{2}(\bar{\sigma}_1 + \bar{\sigma}_2)$  from  $^{31}\text{P}$  in an 85% aqueous solution of orthophosphoric acid ( $\text{H}_3\text{PO}_4$ ) was found to be 233 ppm with a separation of 33 ppm. These shifts were of course isotropic values since the anisotropic components of the shielding tensor are averaged to zero.

We have looked at the response of  $^{31}\text{P}$  to the [1, 3, 2] cycle in powdered  $\text{Zn}_3\text{P}_2$  at 77 °K shifted slightly off-“resonance.” The data were taken at 9.0 MHz and recorded photographically. Since  $T_1 = 3.55$  min at 77 °K these experiments were rather tedious to perform and difficult to align. Figure 7(a) shows a trace for  $\tau = 9.6$   $\mu\text{sec}$ . Increasing the pulse spacing to  $\tau = 12.8$   $\mu\text{sec}$  made no noticeable difference to the response Fig. 7(b). We conclude therefore that we are essentially in the limit  $\tau \rightarrow 0$ .

The composite Fourier transform of two separate experiments is plotted in Fig. 6(b). The horizontal scale which takes account of the scaling factor, indicates real chemical shifts. Calculation of the second moment about the center of gravity of the spectrum gives  $0.07 \text{ G}^2$ . This is somewhat lower than our estimate of the anisotropic chemical-shift contribution to the second moment measured from the double-pulse solid echo response<sup>15,16</sup> which gives  $(0.13 \pm 0.03) \text{ G}^2$ . Some of the difference doubtless arises from our truncation of the wings in the narrowed absorption spectrum.

We notice there is no trace of a resolved doublet with 33 ppm splitting in our spectrum. This is probably due to lack of resolution due to residual broadening. Since  $T_2$  from the free-induction decay is  $\sim 150$   $\mu\text{sec}$  which is much longer than the pulse spacing  $\tau$ , we do not think this broadening can be predominantly dipolar in origin and could be ascribed in part to imperfections in the pulse sequence. However, we are able to estimate the average isotropic part of the shift tensor  $\bar{\sigma}_{\text{av}} = 210 \pm 21$  ppm. The line shape shows some deviation from the powder pattern of an axially symmetric chemical-shift distribution. From Fig. 6(b) we are able to assign tentative values of the average traceless principal components of the shift tensor  $(\Delta\sigma_{11})_{\text{av}}$ ,  $(\Delta\sigma_{22})_{\text{av}}$ , and  $(\Delta\sigma_{33})_{\text{av}}$ . These values are listed in Table I.

During the preparation of this paper a high mag-

netic free-induction decay study of a number of solid phosphorus compounds including  $\text{Zn}_3\text{P}_2$  has been published.<sup>27</sup> The Fourier transformed spectrum for powdered  $\text{Zn}_3\text{P}_2$ , however, shows axial symmetry although the spectral width agrees reasonably well with our data.

Previous multipulse measurements on  $\text{Zn}_3\text{P}_2$  using the modified phase-alternated sequence<sup>6</sup> gave a limiting resolution for phase modulation of the solid echo train corresponding to 84 ppm. The difference between this figure and the expected 33 ppm was ascribed to “a mean anisotropic part of the chemical-shift tensor. . . .” It is clear that our present results are consistent with our previous interpretation.<sup>28</sup>

## C. Interpretation of Results

### 1. Polytetrafluoroethylene

The semiempirical molecular orbital theory of chemical shift developed from earlier work<sup>29,30</sup> by Karplus and Das,<sup>31</sup> Jameson and Gutowsky,<sup>32</sup> and Letcher and Van Wazer<sup>33</sup> forms the basis of our interpretation. In this theory the paramagnetic components of the shielding tensor in the molecular frame are given by

$$\sigma_{ii} = \frac{3}{2} \sigma_0 (\rho_{jj} + \rho_{kk} - \rho_{kk} \rho_{jj}), \quad (21a)$$

$$\sigma_{jj} = \frac{3}{2} \sigma_0 (\rho_{ii} + \rho_{kk} - \rho_{kk} \rho_{ii}), \quad (21b)$$

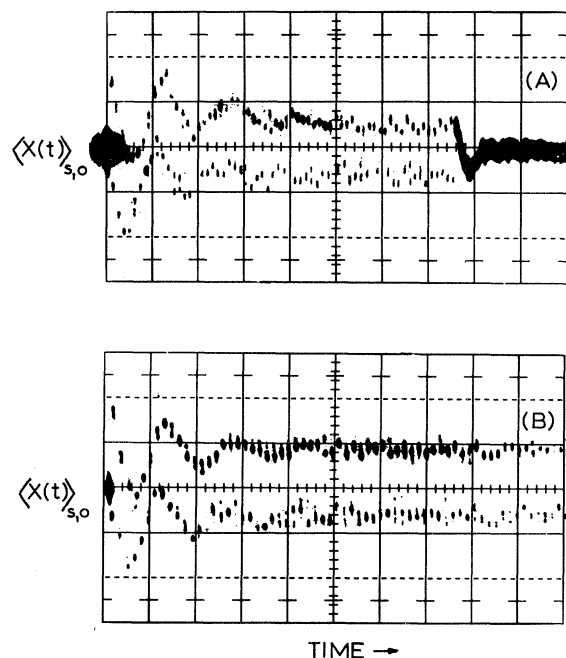


FIG. 7. Photographs of the  $^{31}\text{P}$   $\langle x(t) \rangle_s$  and  $\langle x(t) \rangle_0$  signals in powdered  $\text{Zn}_3\text{P}_2$  at 77 °K in response to the [1,3,2] cycle applied off-resonance by  $\Delta H = 1.5$  G. (a)  $\tau = 9.6$   $\mu\text{sec}$ , and (b)  $\tau = 12.8$   $\mu\text{sec}$ . The horizontal sweep in both traces is 0.5 msec/large division.

$$\sigma_{kk} = \frac{3}{2} \sigma_0 (p_{ii} + p_{jj} - p_{ii} p_{jj}), \quad (21c)$$

where the charge matrix elements  $p_{ii}$  refer to the  $p_i$ -orbital electronic population. Mixed orbital terms  $p_{ij}$  are dropped as well as  $d$ -orbital contributions. A more general analysis including the mixed terms and a  $d$ -orbital contribution has been given by Jameson and Gutowsky.<sup>32</sup> The coefficient  $\sigma_0$  is given as

$$\sigma_0 = -\frac{2}{3} (e^2 \hbar^2 / m^2 c^2) (1/\Delta) \langle 1/r^3 \rangle_p, \quad (22)$$

where  $e$  and  $m$  are the electronic charge and mass, respectively,  $\Delta$  is a mean electronic excitation energy, and  $\langle r^{-3} \rangle_p$  is an average evaluated over the  $p$  orbital.

The isotropic part of the chemical-shift tensor is given by

$$\bar{\sigma} = \frac{1}{3} (\sigma_{ii} + \sigma_{jj} + \sigma_{kk}) = \sigma + \sigma_R, \quad (23)$$

where  $\sigma = \sigma_S - \sigma_R$  is the chemical shift of the sample (S) relative to the same nucleus in some reference compound (R), and  $\sigma_R$  is the absolute paramagnetic shift of the nucleus in the reference compound relative to the unshielded nucleus.

For a completely closed  $p$  shell  $p_{ii} = p_{jj} = p_{kk} = 2$ . This would give zero anisotropy and zero shift. For  $^{19}\text{F}$  one might expect from the ground-state electronic configuration that  $p_{ii} = p_{jj} = 2$  and  $p_{kk} = 1$ , where  $k$  refers to the bond axis. Karplus and Das suggest that one might represent deviations from these conditions as follows:

$$\begin{aligned} p_{ii} &= 2 - \rho_i, & p_{jj} &= 2 - \rho_j, \\ p_{kk} &= 1 + s + I - Is = 1 + \kappa, \end{aligned} \quad (24)$$

where  $\rho_{i,j}$  represents the double-bond character,  $s$  the ( $sp$ ) hybridization parameter, and  $I$  the ionic character of the bond. Using the value of  $\sigma_0 = -863$  ppm obtained by Karplus and Das for fluorine and with  $\rho_i = 0$ , we find our data give best fit for  $\sigma_R = -183$  ppm in which case we obtain  $k = 0.846$  and  $\rho_j = 0.11$

## 2. Zinc Phosphide

Letcher and Van Wazer<sup>33</sup> have applied the Karplus and Das theory as developed by Jameson and Gutowsky to the study of  $^{31}\text{P}$  in a series of symmetrically substituted phosphorus compounds of the type  $MPZ_3$  where  $M$  and  $Z$  are substituents. In the trivalent form the ground-state electronic configuration of the three valence electrons is taken to be the three orthogonal  $p$  orbitals. In their analysis, the  $k$  axis in the molecular reference frame is the  $C_{\infty v}$  symmetry axis. [This corresponds to the (111) axis in the orbital axis reference system.] The angle between the  $P$ - $Z$  bond axis and the  $ij$  plane is  $\eta$  and is by symmetry the same for each bond.

Neglecting  $\pi$ -bonding effects and assuming the  $\sigma$ -bonding orbitals comprise  $s$  and  $p$  orbitals only, they obtain from the orthogonality relationships the following:

$$\alpha^2 + \beta^2 (1 - \frac{3}{2} \cos^2 \eta) = 0, \quad (25a)$$

$$\alpha \alpha' - \beta \beta' \sin \eta = 0, \quad (25b)$$

$$\alpha^2 + \beta^2 = h_A, \quad (25c)$$

$$\alpha'^2 + \beta'^2 = h_M, \quad (25d)$$

where  $\alpha, \beta$  are the amplitudes of the  $s$  and  $p$  orbitals, respectively, for the  $Z$  substituent and  $\alpha', \beta'$  are the corresponding amplitudes for the  $M$  substituent.

The  $Z$ - $P$ - $Z$  bond angle  $\theta$  is related to  $\eta$  by

$$\cos \eta = (2/\sqrt{3}) \sin \frac{1}{2} \theta. \quad (26)$$

From the definition of the charge-bond-order matrix elements  $p_{ij}$ , Letcher and Van Wazer obtain

$$p_{ii} = p_{jj} = \frac{3}{2} \beta^2 \cos^2 \eta, \quad (27a)$$

$$p_{kk} = 3 \beta^2 \sin^2 \eta + \beta'^2. \quad (27b)$$

If we put  $\theta = 90^\circ + \phi$ , where  $\phi$  is a small deviation from orthogonality of the  $Z$ - $P$ - $Z$  bond angle, we obtain

$$\cos \eta = \sqrt{\frac{2}{3}} (\cos \frac{1}{2} \phi + \sin \frac{1}{2} \phi) = \sqrt{\frac{2}{3}} \epsilon. \quad (28)$$

For triply substituted compounds  $h_M = 2$ , the two  $p$  electrons for a closed pair thus residing in the phosphorus orbital. The fraction of charge residing in the phosphorus atom in the  $P$ - $Z$  bond is taken to be the Coulson expression<sup>34</sup>

$$\begin{aligned} h_A &= 1 + 0.16(E_P - E_A) + 0.035(E_P - E_A)^2 \\ &= 1 + I, \end{aligned} \quad (29)$$

where  $E_\alpha$  is the electronegativity of the element  $\alpha$ . Substituting the above expressions into Eqs. (21a)–(21c) we obtain

$$\begin{aligned} \sigma_{ii} &= \sigma_{jj} \\ &= \frac{3}{2} \sigma_0 \left\{ 1 + I - I \left[ 3(I+1) \left( \frac{1}{\epsilon^2} - \frac{2}{3} \right) + 6(1 - 1/\epsilon^2) \right] \right\}, \end{aligned} \quad (30a)$$

$$\sigma_{kk} = \frac{3}{2} \sigma_0 (1 - I^2). \quad (30b)$$

Using the electronegativity values<sup>35</sup> for phosphorus of  $E_P = 2.1$  and a value for zinc of 1.66 gives  $I = 0.07$ .

The structure of  $\text{Zn}_3\text{P}_2$  is quite complicated,<sup>36,37</sup> there being 24 Zn atoms and 16 P atoms in the tetragonal unit cell. The 24 Zn atoms comprise three crystallographically distinct groups of 8, while the 16 P atoms comprise one group of 8, and two groups of 4. The zincs are each surrounded by a deformed tetrahedron of P atoms. Each P atom has six zinc neighbors with no simple symmetry.

The isotropic chemical shift of phosphine ( $\text{PH}_3$ ) relative to  $\text{H}_3\text{PO}_4$  is 240 ppm. In this material the P-H bond length is 1.473 Å and the bond is strongly covalent. The H-P-H bond angle is 93.5°. Zinc phosphide has a similarly large isotropic chemical shift. However, the Zn-P bond lengths are substantially longer lying between 2.28 and 2.77 Å leading to some doubt in the character of the bond. Some phosphorus compounds, normally reckoned to be covalent, do however have bond lengths of the order of 2 Å.

In trying to interpret our results we have considered  $\text{Zn}_3\text{P}_2$  as being a covalent solid. Each phosphorus is supposed connected to three Zn atoms in such a way as to keep the bond angles equal (if possible) and close to 90°. Calculation of the actual bond angles gives an average of 111.2° and is close to the tetrahedral angle of 109.5°. Thus although our model deviates from reality it allows straightforward application of the existing theory. One consequence of this is that the chemical shielding tensor is always axially symmetric. From our data we assign a mean perpendicular component of chemical shift

$$\sigma_{\perp} = \frac{1}{2}[(\sigma_{ii})_{\text{av}} + (\sigma_{jj})_{\text{av}}]$$

and hence an asymmetry parameter  $\Delta\sigma = \sigma_{\perp} - \sigma_{\parallel}$ . Equations (23) and (30) can then be solved simultaneously for a Zn-P-Zn bond angle of 110° to give  $\sigma_0 = -1940$  ppm and  $\sigma_R = 2990$  ppm. These values of the constants differ considerably from those deduced by Letcher and Van Wazer based on studies of the isotropic chemical shifts of a number of triply substituted phosphines. Inclusion of  $\pi$ -bonding orbitals could reduce this discrepancy. However, we suspect that such a simple readjustment of the theory to give agreement for the isotropic shift would not explain the anisotropy. The important point is that measurements of both the isotropic and anisotropic parts of the shielding tensor give a mutually compatible set of constants without reference to other compounds. It is interesting to note that with our values of the constants, a decrease in the bond angle of 10° reduces the isotropic shielding tensor by 55 ppm. This sensitivity to bond angle<sup>38</sup> could thus be partly responsible for the isotropic shift doublet reported elsewhere.<sup>25,26</sup>

## V. APPARATUS

The spectrometer is a hybrid rig using mainly transistorized control and rf gating logic at the low-power end. Although these components are broad band, the equipment over all is essentially fixed frequency due to bandwidth limitations of the intermediate and final rf amplifiers and operates at 9.0 MHz. The final transmitter output is of conventional tube design producing about 5-kW peak

power pulses in a cross-coil probe.

A block diagram of the equipment is shown in Fig. 8 and illustrates the scheme of rf logic used. The solid-state broad-band rf gates are fairly fast-rise-time ( $\sim 10$  nsec) high-attenuation ( $\sim 120$  dB) transmission gates and will be described together with the broad-band solid-state phase shifters elsewhere.<sup>39</sup> The phase shifters are switched and the rf gate-width control pulses are triggered directly from a Honeywell 316 computer. The pulse patterns for any cycle, the pulse-train length and the repetition rate are programed entirely by software. All timings are therefore related to integral multiples of the machine cycle time, 1.6  $\mu\text{sec}$ . We have not found this constraint to be a hindrance so far. For  $\tau < 4.8$   $\mu\text{sec}$ , our present method for generating pulse patterns would be limited to software programs which could not accommodate the possibility of computer sampling of the signal.

In our experiments the internal computer clock was used directly for all timing. For greater timing accuracy this could of course be replaced by an external timing pulse derived from a master crystal clock. This would also ensure pulse coherence, which we found to be necessary in all our experiments. In our case pulse coherence is achieved by a straightforward retiming circuit (see Fig. 8).

The sample probe consists of a cylindrical Helmholtz cross-coil assembly following the design used by Lurie and Slichter.<sup>40,41</sup> Signal reception is performed using a standard-design synchronously tuned broad-band receiver, modified to include phase-sensitive detection. In order to improve the recovery time of the system active switching at the receiver input is employed. Use of an FET  $\pi$  switch<sup>42</sup> has enabled us to reduce the resolution time including the 1.1- $\mu\text{sec}$  pulse to 8.0  $\mu\text{sec}$ . This time is controlled by transmitter coil ringing and could be further reduced by heavier damping or active switching of the transmitter coil.

## VI. PHASE EFFECTS

### A. Phase Compensation

In addition to compensation for finite rf pulse width and rf field inhomogeneity it is possible to design cycles in which the systematic errors in the 90° and 180° phase shifters are self-correcting.<sup>14</sup> Because of the increased complexity of fully symmetrized compensated cycles we feel that the full experimental realization of these cycles will ultimately depend on the ease with which these cycles can be set up. Phase compensation of the type discussed here should make these cycles less critical to exact phase settings and hence simpler to adjust.

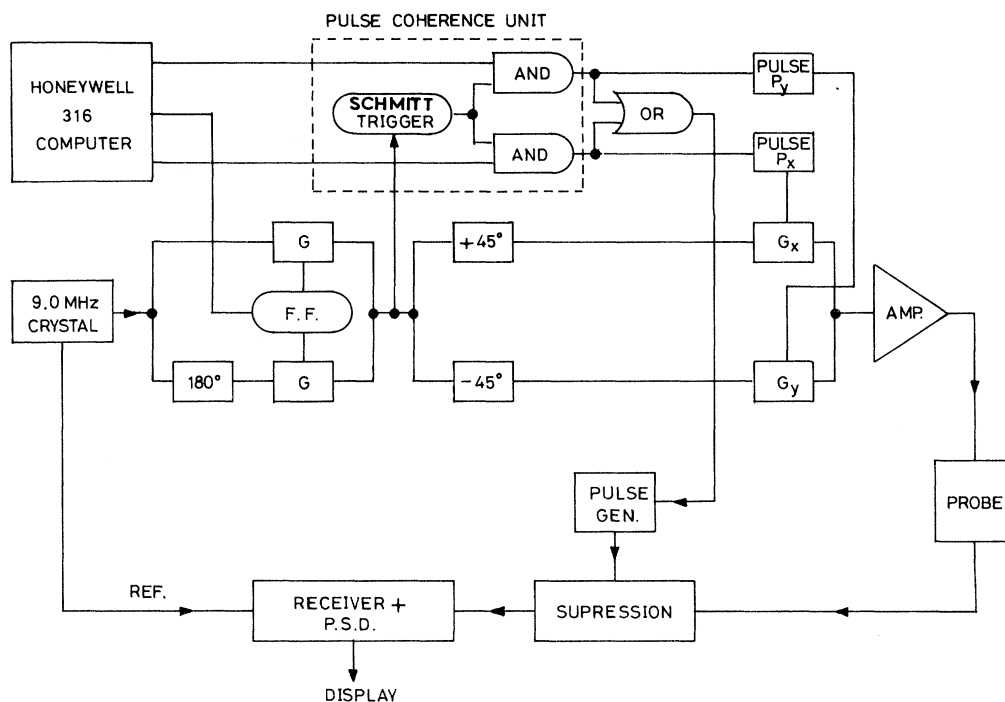


FIG. 8. Block diagram of the computer-controlled spectrometer. F. F. denotes a bistable flip-flop circuit and G denotes an rf transmission gate.

To understand the operation we refer to Fig. 8. The  $180^\circ$  phase modulator is common to both the  $x$  and the  $y$  channel. Since it can be set only to a certain accuracy there will be, in general, a phase error  $\phi_1$  associated with this phase shifter. This introduces modulation of the transient response in competition to resonance shifts hence limiting the resolution of small field shifts. Cumulative phase errors can be removed in first order by employing two phase modulators in series as in Fig. 9. The second modulator will of course introduce a phase error  $\phi_2$ .

We denote an rf pulse which has a  $180^\circ$  phase shift derived from the first phase modulator as  $P_{\pm\alpha}$  and from the second as  $P_{\pm\alpha}^+$ . It is evident that in any cycle of rf pulses, systematic phase errors introduced in one cycle can be removed in first order in the second cycle by routing all rf pulses in this cycle through the second phase modulator. To maintain the basic properties of the cycle, however, it is clearly necessary to pass the phase complement of the first cycle through the second phase shifter. In this way both errors  $\phi_1$  and  $\phi_2$  vanish in first order with no special adjustment. The frequency scaling factor, of course, remains the same as for the uncompensated cycle.

As a simple example we take the phase-alternated cycle. The phase-compensated form of this is

$$P_{-y} - (\tau - P_x - 2\tau - P_{-x} - 2\tau - P_{-x}^+ - 2\tau - P_x^+ - \tau)_n.$$

Examples of this sequence are shown in Fig. 10 applied to  $^1\text{H}$  in water. The response in the uncompensated case for  $\Delta\omega = 0$  and  $\phi = 0$ , Fig. 10(a), is compared with the compensated form with  $\Delta\omega = 0$  and  $\phi = 0.35$  rad [Fig. 10(b)] and is seen to be substantially independent of phase error up to  $\phi = 10^\circ$ . The latter part of each trace is the normal free-induction decay which in both cases is seen to be monotonic. For the same phase error ( $\sim 10^\circ$ ) the compensated response slightly shifted from resonance ( $\Delta\omega = 4.68$  krad  $\text{sec}^{-1}$ ) is shown in Fig. 10(c) and the scaling factor is found to be the same as that for the uncompensated cycle for the same resonance shift, in

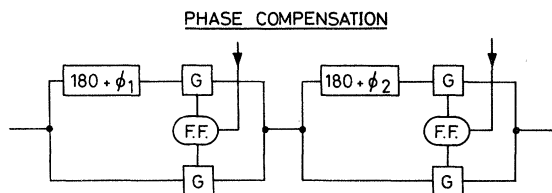


FIG. 9. Double-series  $180^\circ$  phase modulator. F. F. denotes a bistable flip-flop circuit and G denotes an rf transmission gate.

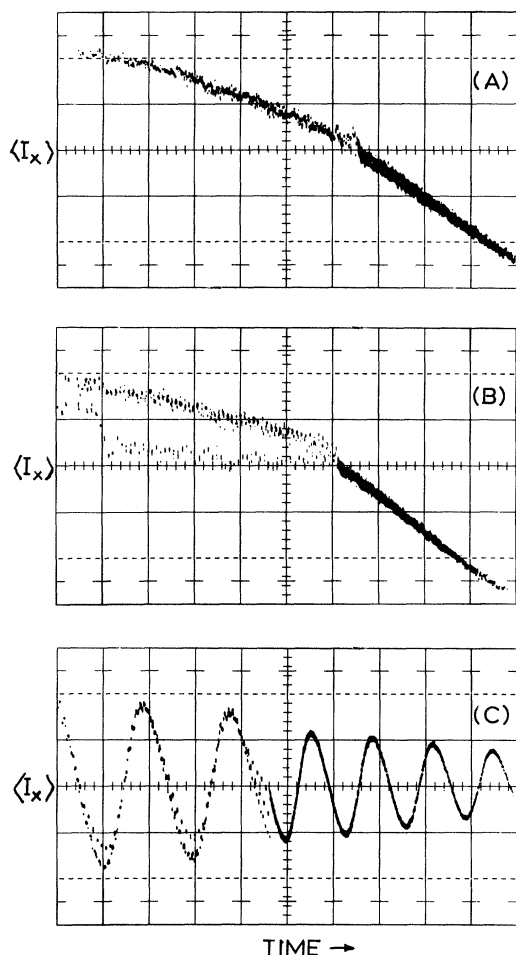


FIG. 10. Photographs showing phase compensation of the signal response of  $^1\text{H}$  in water at room temperature following a phase-alternated multipulse sequence. (a) Uncompensated  $P_y - (\tau - P_x - 2\tau - P_x - \tau)_n$  sequence with  $\Delta\omega = 0$  and  $\phi = 0$ , (b) compensated sequence  $P_y - (\tau - P_x - 2\tau - P_x - 2\tau - P_x^+ - 2\tau - P_x^+ - \tau)_n$  with  $\Delta\omega = 0$  and  $\phi = 0.35$  rad, and (c) as in (b) above but off-resonance by  $\Delta\omega = 4.68$  krad  $\text{sec}^{-1}$ . Horizontal sweep in all photographs is 1.0 msec/large division and  $\tau = 12$   $\mu\text{sec}$ . Note the latter part of each trace is the normal free-induction decay.

this case a factor of 1.46.

It is clear that this procedure for phase compensation also corrects for any systematic phase errors in the alignment of phase quadrature between the  $x$  and  $y$  channels in more complicated cycles. As it happens, all six forms of the reflection-symmetry cycle and their compensated versions are self-correcting for this type of phase error.

Phase transients caused by applying stepped rf pulses to tuned amplifiers, phase shifts due to thermal effects, particularly in long pulse trains, and random phase errors cannot be compensated

by the above scheme. The first of these errors can be reduced by pulse coherence, especially if the gates are arranged to open at an rf zero crossing, and also by careful tuning of the rf stages. Thermal effects can be reduced by conservatively rating all resistive components and active devices.

#### B. Amplitude-Modulation Effects

In the phase-alternated experiment  $P_y - (\tau - P_x - 2\tau - P_x - \tau)_n$  carried out in a liquid with a Gaussian inhomogeneous distribution of Larmor frequencies, the response at resonance is a monotonic decay with a time constant longer than the usual inhomogeneous free-induction decay value by the factor  $\sqrt{2}$  in the limit of  $\tau \rightarrow 0$  and with the real time  $t = 4n\tau$  finite,  $n$  integer. Waugh *et al.*<sup>3</sup> have calculated an exact expression for the response to a phase-alternated sequence of a liquid with spin  $\frac{1}{2}$ .

In a modified form of this sequence, in which the phase of alternate pulses is varied from  $180^\circ$  by a small phase angle  $\phi$ , we noticed in some solids that the solid echo train decay time constant could be increased. In homogeneously broadened liquids and motionally narrowed solids such as lithium metal at room temperature, the observed decrease in the damping was even more dramatic. A phase angle  $\phi = 0.05$  rad caused the onset of beats and a reduction in the damping. The damping reached a minimum at  $\phi = 0.156$  rad at which value it remained constant for further increase in  $\phi$ .

We have evaluated the response for a set of non-interacting spins  $\frac{1}{2}$  including the phase deviation  $\phi$  and obtain

$$\frac{\langle I_x \rangle}{\langle I_x \rangle_0} = \sum_i \frac{2}{1 + A_i^2} \times \left\{ \frac{1}{2} \sin^2 \frac{1}{2} \phi + \frac{1}{4} [\cos \frac{1}{2} \phi + 1 + 2A_i^2] \cos 2n\alpha_i \right\}, \quad (31a)$$

where

$$A_i = \frac{\sin(\Delta_i \tau + \frac{1}{2} \phi)}{\sin(\Delta_i \tau - \frac{1}{2} \phi)} \cos(\Delta_i \tau - \frac{1}{2} \phi) \quad (31b)$$

and the resonance shift  $\Delta_i = \delta_i + \Delta\omega$ . The angle  $\alpha_i$  is defined by

$$\tan \alpha_i = \frac{\sin(\Delta_i \tau - \frac{1}{2} \phi)(1 + A_i^2)^{1/2}}{\cos(\Delta_i \tau - \frac{1}{2} \phi) \cos(\Delta_i \tau + \frac{1}{2} \phi)}. \quad (31c)$$

In the special cases (i)  $\phi = 0$ ,  $\tau \rightarrow 0$  and (ii)  $\Delta_i = 0$ ,  $\phi \rightarrow 0$ , Eq. (31a) reduces to

$$\langle I_x \rangle / \langle I_x \rangle_0 = \sum_i \cos 2n\alpha_i, \quad (32)$$

where for case (i)  $\alpha_i \rightarrow \Delta_i \tau \sqrt{2}$  and for case (ii)  $\alpha_i \rightarrow -\phi / \sqrt{2}$ . Equation (31a) has been evaluated for a Gaussian inhomogeneous static magnetic field distribution of the form

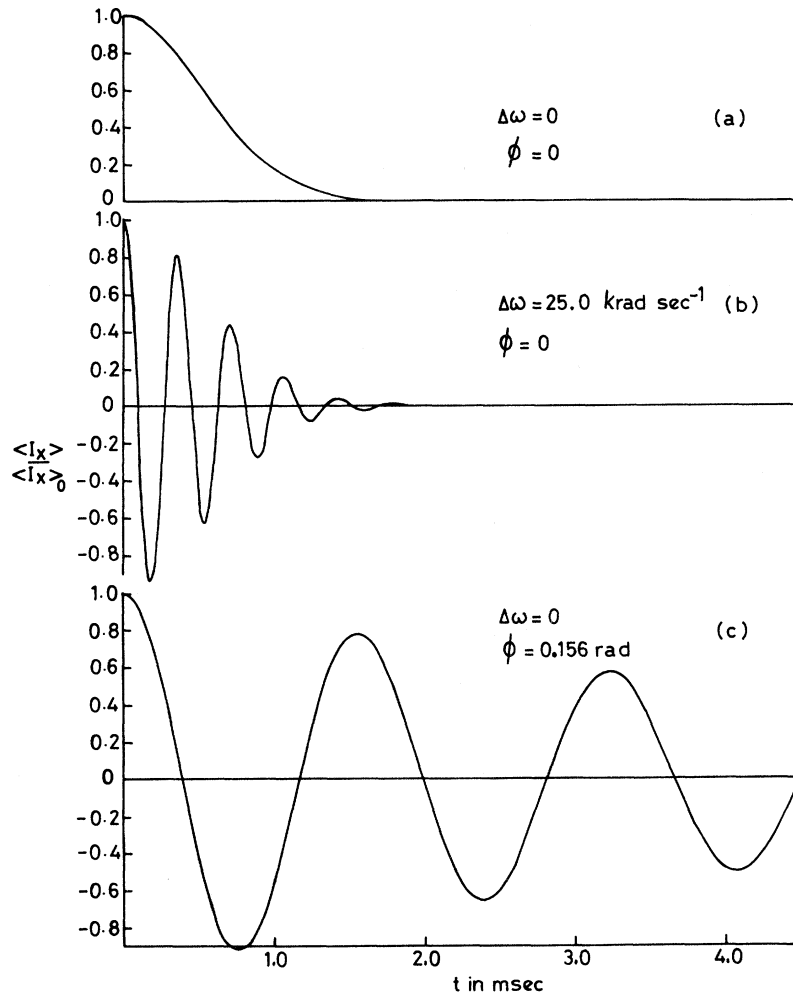


FIG. 11. Theoretical response [Eq. (31a)] of noninteracting spins- $\frac{1}{2}$  to the phase-alternated sequence  $P_y - (\tau - P_x - 2\tau - P_x - \tau)_n$ , evaluated for a Gaussian inhomogeneous distribution of Larmor frequencies (see text) and with  $\tau = 15 \mu\text{sec}$ . (a) On-resonance,  $\Delta\omega = 0$  and phase error  $\phi = 0$ . This shows the inhomogeneous decay, (b) off-resonance by  $\Delta\omega = 25.0 \text{ krad sec}^{-1}$  and phase error  $\phi = 0$ . Note that the wiggles are contained within the inhomogeneous decay envelope, and (c) on resonance,  $\Delta\omega = 0$  but with phase error  $\phi = 0.156 \text{ rad}$ . The damping is significantly reduced.

$$f(\omega) = (\pi/2a^2)^{1/2} e^{-\omega^2/2a^2}$$

with  $a = 2.62 \times 10^3 \text{ rad sec}^{-1}$  corresponding to the observed inhomogeneity in the free-induction decay. The results for  $\Delta\omega = \phi = 0$ ;  $\Delta\omega = 25.0 \text{ krad sec}^{-1}$ ,  $\phi = 0$ ; and  $\Delta\omega = 0$ ,  $\phi = 0.156 \text{ rad}$  are plotted in Fig. 11 for  $\tau = 15 \mu\text{sec}$ . Notice that for on-phase and off-resonance the wiggles are contained within the inhomogeneous field damping envelope. For nonzero phase, however, the effective damping is substantially decreased. In Fig. 12 we give actual experimental results for  $^1\text{H}$  in water with  $\tau = 15 \mu\text{sec}$ .

Although Eq. (31a) is exact, except for finite pulse-width effects and rf inhomogeneity, it is not immediately obvious from its form that decreased damping would result from including a phase term  $\phi$ . It is true, of course, that for a perfect homogeneous static field and in the absence of spin-lattice relaxation the response signal would not decay for any  $\phi$ . In the present circumstance one might naively expect that the phase wiggles should be

amplitude modulated in exactly the same way as those for the off-resonance case, that is to say, contained within the inhomogeneous decay envelope. That this conclusion is wrong is clear from the experimental results and detailed computer evaluation of Eq. (31a).

The average Hamiltonian approach gives essentially the cosine term only in Eq. (31a) with  $\alpha_i = [2(\Delta_i\tau)^2 + \frac{1}{2}\phi^2]^{1/2}$ . Detailed computer evaluation in this case shows that damped and highly distorted phase wiggles do persist beyond the inhomogeneous decay time, but they bear little resemblance to the smooth regular wiggles observed experimentally, Fig. 12.

The main difference between the average Hamiltonian calculation and the exact expression [Eq. (31a)] is the appearance of the  $\frac{1}{2} \sin^2 \frac{1}{2} \phi$  term and cosine amplitude factor. It would seem that their exact form plays a significant role in the actual shape and damping of the phase wiggles, even though from the magnitude of  $\phi$  and  $\Delta_i\tau$  one expects to be in the average Hamiltonian limit. As

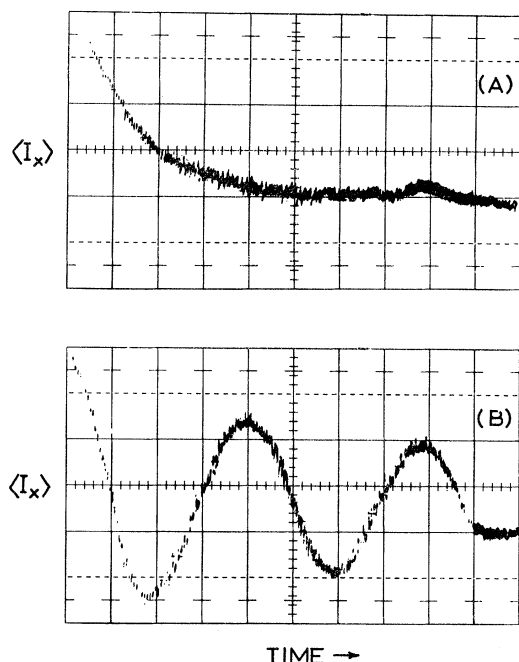


FIG. 12. Photographs of the response of  $^1\text{H}$  in water to the phase-alternated sequence  $P_y - (\tau - P_x - 2\tau - P_x - \tau)_n$  applied at resonance with  $\tau = 15 \mu\text{sec}$ . In (a)  $\phi = 0$  and in (b)  $\phi = 0.156 \text{ rad}$ . Horizontal sweep is  $0.5 \text{ msec}$ /large division.

evidence for this last point we can look to the periodicity of the phase wiggles in the evaluated expression [Eq. (31a)] which does agree fairly well with the average Hamiltonian limit [Eq. (32), case (ii)]. The inhomogeneous decay with  $\phi = 0$ , [Fig. (11a)] also agrees in the same limit. Calculations in the average Hamiltonian limit show that phase wiggles similar to those described above should occur in all forms of the reflection-symmetry cycle.

## VII. CONCLUSIONS

We have demonstrated experimental realization of one form of the reflection-symmetry cycle and shown that in either its elementary form or its compensated form it is capable of resolving chemical-shift tensors in solids which are normally hidden by the dipolar interaction. By way of an example of the application of these cycles, some preliminary data on  $^{19}\text{F}$  in  $(\text{C}_2\text{F}_4)_n$  and  $^{31}\text{P}$  in powdered  $\text{Zn}_3\text{P}_2$  is presented and discussed. These data, obtained by a computer-controlled spectrometer, are single shot and could be greatly improved by signal averaging.

The effect of phase errors in the setting up of the pulse sequences is discussed and the principle of phase compensation is demonstrated experimentally on a phase-alternated sequence. Another striking effect of introducing a phase error is the reduction of damping beyond the  $\sqrt{2}$  effect in a phase-alternated sequence. Detailed calculation for noninteracting spins  $\frac{1}{2}$  is shown to predict the observed experimental behavior. The predictions of the simple average Hamiltonian theory, while correct for the periodicity of phase wiggles, are at variance with the observed facts regarding the shape of the response signal and its damping.

## ACKNOWLEDGMENTS

We wish to thank our colleagues Professor E. R. Andrew, Dr. W. Derbyshire, and Dr. A. N. Garroway for reading the manuscript and making a number of valuable suggestions for its improvement. We also wish to thank Dr. J. L. Carolan for writing the Fourier-transform computer program and Dr. W. S. Hinshaw for writing the powder-line-shape program and also making a number of preliminary measurements on zinc phosphide. We are grateful to the Science Research Council for providing research studentships for two of us (M. J. O. and D. C. S.).

\*Research supported by a Science Research Council Equipment Grant.

†Present address: Physics Department, Fourah Bay College, University of Sierra Leone, West Africa.

<sup>1</sup>E. R. Andrew, A. Bradbury, and R. G. Eades, *Arch. Sci. (Geneva)* **11**, 223 (1958); *Nature* **182**, 1659 (1958); **183**, 1802 (1959).

<sup>2</sup>I. J. Lowe, *Phys. Rev. Letters* **2**, 285 (1959).

<sup>3</sup>J. S. Waugh, C. H. Wang, L. M. Huber, and R. L. Vold, *J. Chem. Phys.* **48**, 662 (1968).

<sup>4</sup>J. S. Waugh, L. M. Huber, and U. Haeberlen, *Phys. Rev. Letters* **20**, 180 (1968).

<sup>5</sup>U. Haeberlen and J. S. Waugh, *Phys. Rev.* **175**, 453 (1968).

<sup>6</sup>P. Mansfield and K. H. B. Richards, *Chem. Phys. Letters* **3**, 169 (1969); **6**, 123 (1970).

<sup>7</sup>J. D. Ellett, U. Haeberlen, and J. S. Waugh, *Polymer Letters* **7**, 71 (1969).

<sup>8</sup>U. Haeberlen and J. S. Waugh, *Phys. Rev.* **185**, 420 (1969).

<sup>9</sup>J. D. Ellett, U. Haeberlen, and J. S. Waugh, *J. Am. Chem. Soc.* **92**, 411 (1970).

<sup>10</sup>M. Mehring, R. G. Griffin, and J. S. Waugh, *J. Chem. Phys.* **55**, 746 (1971).

<sup>11</sup>L. M. Stacey, R. W. Vaughan, and D. D. Elleman, *Phys. Rev. Letters* **26**, 1153 (1971).

<sup>12</sup>P. Mansfield, *Phys. Letters* **32A**, 485 (1970).

<sup>13</sup>P. Mansfield, in *Progress in Nuclear Magnetic Resonance Spectroscopy*, edited by J. W. Emsley, J. Feeney, and L. H. Sutcliffe (Pergamon, Oxford, 1971), Vol. 8, p. 41.

<sup>14</sup>P. Mansfield, *J. Phys. C* **4**, 1444 (1971).

<sup>15</sup>J. G. Powles and J. H. Strange, *Proc. Phys. Soc. (London)* **82**, 6 (1963).

<sup>16</sup>P. Mansfield, *Phys. Rev.* **137**, A961 (1965).

<sup>17</sup>M. Lee and W. I. Goldberg, *Phys. Rev.* **140**, A1261

(1965).

<sup>18</sup>C. P. Slichter, *Principles of Magnetic Resonance* (Harper and Row, New York, 1963).<sup>19</sup>P. Mansfield, *Phys. Rev.* **151**, 199 (1966).<sup>20</sup>U. Haebleren, J. D. Ellett, and J. S. Waugh, *J. Chem. Phys.* **55**, 53 (1971).<sup>21</sup>A. Abragam, *The Principles of Nuclear Magnetism* (Clarendon, Oxford, 1961).<sup>22</sup>H. Goldstein, *Classical Mechanics* (Addison-Wesley Reading, Mass., 1956), p. 109.<sup>23</sup>N. Bloembergen and T. J. Rowland, *Acta Met.* **1**, 731 (1953).<sup>24</sup>N. Bloembergen and T. J. Rowland, *Phys. Rev.* **97**, 1679 (1955).<sup>25</sup>E. R. Andrew and V. T. Wynn, *Proc. Roy. Soc. (London)* **A291**, 257 (1966).<sup>26</sup>H. Kessemeier and R. E. Norberg, *Phys. Rev.* **155**, 321 (1967).<sup>27</sup>M. G. Gibby, A. Pines, W.-K. Rhim, and J. S. Waugh, *J. Chem. Phys.* **56**, 991 (1972).

<sup>28</sup>Computer simulation studies of the phase wiggles on-resonance (see Sec. VI) in a spin system broadened solely by a symmetric distribution of resonance frequencies indicate deviation from simple cosine dependence for small  $\phi$  in a similar way to that observed in  $\text{Zn}_3\text{P}_2$ . The graph of average modulation angular frequency, calculated from the first and second zero crossing, versus  $\phi/2\tau$  intersects the line  $\omega = \phi/2\tau$  at about  $0.60a$ , where  $a$  is the half-width of the inhomogeneous distribu-

tion. Thus it seems that our previous experiments were indeed measuring essentially the width of the inhomogeneous distribution, that is to say, the anisotropy.

<sup>29</sup>N. F. Ramsey, *Phys. Rev.* **77**, 567 (1950); **78**, 699 (1950).<sup>30</sup>A. Saika and C. P. Slichter, *J. Chem. Phys.* **22**, 26 (1954).<sup>31</sup>M. Karplus and T. P. Das, *J. Chem. Phys.* **34**, 1683 (1961).<sup>32</sup>C. J. Jameson and H. S. Gutowsky, *J. Chem. Phys.* **40**, 1714 (1964).<sup>33</sup>J. H. Letcher and J. R. Van Wazer, *J. Chem. Phys.* **44**, 815 (1966); **45**, 2916 (1966); **45**, 2926 (1966).<sup>34</sup>C. A. Coulson, *Valence* (Clarendon, Oxford, 1953), p. 132.<sup>35</sup>W. J. Moore, *Physical Chemistry* (Longmans Green, London, 1966), p. 546.<sup>36</sup>M. von Stackelberg and R. Paulus, *Z. Physik Chem.* **28B**, 427 (1935).<sup>37</sup>R. W. G. Wyckoff, *Crystal Structures* (Interscience, New York, 1964), Vol. VII, p. 33.<sup>38</sup>See also D. Purdela, *J. Mag. Res.* **5**, 23 (1971).<sup>39</sup>T. Baines and P. Mansfield (unpublished).<sup>40</sup>F. M. Lurie and C. P. Slichter, *Phys. Rev.* **133**, A1108 (1964).<sup>41</sup>D. M. Ginsberg and M. J. Melchner, *Rev. Sci. Instr.* **41**, 122 (1970).<sup>42</sup>P. K. Grannell, P. Mansfield, M. J. Orchard, and D. C. Stalker (unpublished).

## Knight-Shift Anisotropy in Cubic Crystals<sup>\*†</sup>

A. Rubens B. deCastro<sup>‡</sup> and R. T. Schumacher

*Department of Physics, Carnegie-Mellon University, Pittsburgh, Pennsylvania 15213*

(Received 21 July 1972)

A general calculation of the Knight shift in metals with spin-orbit interaction is presented. For terms involving the electron-nuclear contact interaction the spin-orbit interaction was included to second order and is shown to result in anisotropy of the Knight shift even in cubic metals. Our formalism for electron-nuclear dipole interaction with spin-orbit coupling also yields anisotropy in cubic metals and reduces in the tight-binding limit to the result previously obtained by Boon. Nuclear-magnetic-resonance measurements on single crystals of the cubic metals lead and platinum have shown the anisotropy in our samples to be less than, respectively, 3.4 and  $1.5 \times 10^{-4}$  of the isotropic shifts. The upper limit for lead is half the anisotropy in lead reported by Schratter and Williams.

### I. INTRODUCTION

The Knight shift is normally taken to be magnetic shielding of a nucleus in a metal by the surrounding electronic magnetic moments and their orbital currents. If  $\Delta\vec{B}$  is the internal field seen by the nucleus, and the external field  $\vec{B}_0$  is applied in the  $z$  direction, then the Knight shift  $K$  is

$$K = \Delta B_z / B_0.$$

In a (hypothetical) noncrystalline, isotropic substance, the direction of the internal field  $\Delta\vec{B}$  is the same as the direction of the applied field  $\vec{B}_0$ . In

a real metal the nature of the electronic wave functions is determined by the periodic crystalline potential; the orbital currents and, if there is spin-orbit coupling, the spin direction are sensitive to the nature of the crystal potential, and consequently, in general,  $\Delta\vec{B}$  is not parallel to  $\vec{B}_0$ . The consequences are familiar in noncubic metals, where the Knight shift has long been known to be anisotropic. It is less obvious that the Knight shift can be anisotropic in cubic metals as well. That it can was first (to our knowledge) pointed out by Boon,<sup>1</sup> who displayed a formula for the anisotropic part of the shift due to the combined effects of